



A hybrid numerical and imaging approach for characterizing defects in composite structures



Rani F. Elhajjar^{a,*}, Seyedmohammad S. Shams^a, Gabor J. Kemeny^b, Gina Stuessy^b

^a College of Engineering & Applied Science, University of Wisconsin, Milwaukee, WI 53211, USA

^b Middleton Spectral Vision, 8505 University Green, Middleton, WI 53562, USA

ARTICLE INFO

Article history:

Received 21 July 2015

Received in revised form 19 October 2015

Accepted 24 October 2015

Available online 28 October 2015

Keywords:

A. Polymer-matrix composites (PMCs)

B. Defects

C. Damage mechanics

D. Optical microscopy

ABSTRACT

In this study, a hybrid approach coupling hyperspectral near infrared imaging with a progressive finite element method is proposed for characterization of the elastic and failure response of composites with non-uniform variations of the wrinkles profile through the thickness and across the structure dimensions. In this approach, hyperspectral near infrared spectroscopy is used to create a 3D profile of the surface resin pockets with the capability of measuring resin thickness from approximately 125 to 2500 μm . These resin pockets are directly correlated to underlying ply level wrinkling as confirmed by optical microscopy. The 3D mapped resin plane obtained from the hyperspectral imaging is used to morph a ply-by-ply finite element model of a carbon-fiber/epoxy resin laminated plate using a progressive damage failure methodology. The results show the capability of the hybrid method to predict the structural response in laminated composites containing spatially distributed and non-uniform ply-level wrinkling.

© 2015 Elsevier Ltd. All rights reserved.

1. Introduction

Composite structures in practice can be subject to various types of defects during manufacturing. Such defects can serve as initiation sites for matrix cracking, fiber kinking, fiber/matrix debonding and delamination. Of the possible defects, ply-level out-of-plane waviness or wrinkling can lead to the highest degradation of mechanical properties [1–4] and is the most challenging of defects to detect using conventional approaches. Ply waviness can be caused by wrinkles in bagging or non-uniform consolidation pressure, interactions with other layers or ply drop-offs. Processing parameters including length of cure, cooling rate, and tool plate material can also influence the development of wrinkles in the laminates [5].

Current analysis methods for composites with defects are limited by the ability of nondestructive methods to adequately and economically characterize the defect levels in the structure. Sutcliffe et al. [6] used an X-ray image analysis technique to determine the fiber waviness. This technique provided good agreement with results from the polished prepreg (preimpregnated fibers) samples. Similarly, Nikishkov et al. [7] proposed a method for automated generation of finite element meshes for unidirectional composites with waviness defects using X-ray computed tomography. Pain

and Drinkwater [8] used an ultrasonic array to extract the scattering of the interior of the composite structure. Pulsed terahertz response of the composite is shown to provide clear indications of the fiber waviness [9] but characterization of wrinkle levels continues to be an area of concern and is likely to be limited by a variety of factors such as the stacking sequence and the thickness of the structure in question. Ultrasonic characterization methods are difficult to interpret because elastic wave propagation is highly dependent on stacking sequence effects and interactions with other defects, such as porosity, which can occur at the same time as wrinkle defects. The computed tomography methods previously discussed are limited to testing specimens of small sizes and are currently not practical for many types of composite structures.

In the absence of reliable stochastic or multi-physics models that account for manufacturing, it is not possible at this point to accurately predict the locations where defects occur before manufacturing. Even if the wrinkle defect is visible, it is not currently possible to reliably determine its depth non-destructively using methods that are commonly used, such as ultrasonic inspection. In other cases, excess resin on the composite surface might result from a wrinkle in the bagging material, so there is no underlying composite feature. NDI methods based on ultrasound can detect resin pockets in excess of 1000 μm but cannot typically measure pockets that are less than 1000 μm deep. Thermoelastic stress analysis methods have also been proposed to identify resin pockets and wrinkles, but these require a cyclic application of load [10].

* Corresponding author. Tel.: +1 414 229 3647; fax: +1 414 229 6958.

E-mail address: elhajjar@uwm.edu (R.F. Elhajjar).

Thus there exists the need for robust, portable and accurate methods for providing identification and depth measurement of wrinkles in composite structures.

Chemometric data processing methods can be used to characterize the relationship between the spectra and the resin thickness and provide the correlation to predict a point-by-point local resin thickness and thus produce thickness maps of the scanned resin surface. Recent advances in hyperspectral near infrared (NIR) sensing and data processing technologies have made real-time infrared methodologies a viable solution for accurate analysis of composite structures. NIR imaging can accurately measure surface resin on composite materials from 125 to 2500 μm thick, detecting virtually all resin pockets, resin-filled surface wrinkles and other surface resin features [11]. The resin-rich areas on the surface are usually an indicator that wrinkles are affecting some or all of the plies in a laminate stack.

In this study, we propose using NIR hyperspectral imaging and progressive damage finite element analysis for advanced distributed damage characterization in composite structures. Our approach overcomes the obstacles facing accurate mechanical analysis of the structure as it is built without simplifying assumptions of defect levels. The progressive modeling approach is based on the Hashin–Puck's continuum damage criteria and cohesive layers. A finite element mesh generation technique with the capability of meshing layers separately has been developed to transform the resin thickness maps to a finite element mesh with a ply-by-ply representation including cohesive layer failure interfaces in between the plies. The proposed method is demonstrated on a continuous plain weave fabric carbon fiber/epoxy laminate.

2. Method

In our proposed method, a push-broom near infrared (NIR) hyperspectral imaging approach is used to scan the composite structure and produce a map of the resin depth on the surface. This map is subsequently used to generate a morphed finite element model corresponding to the non-uniform wrinkling in the structure. A progressive damage-based finite element method is used to predict the elastic and failure response at any desired location. The result is not only a defect map, but also a detailed structural health assessment of the distributed damage due to the non-uniform ply waviness in the structure. The steps involved in this method are comprised of the following:

- (1) In the push-broom NIR hyperspectral imaging approach, a line of pixels is measured and the sample is moved along a path that is perpendicular to the imaging line. The push-broom approach to imaging is capable of high spatial resolution to completely define the resin features by generating a 3D profile of the resin features on the surface of the composite structure (Fig. 1).
- (2) The 3D profile of the resin is subsequently used to modify the finite element mesh of the structure in question. Information from the resin profile is used to introduce wrinkles from the 3D surface resin map. The mesh-morphing program is capable of adjusting the thickness of the plies to the newly imposed constraints. Optical microscopy confirms the link between wrinkle depth and the resin thickness on the surface.
- (3) A progressive finite element method comprising continuum damage zone theory and cohesive layers is used to compute the structural stiffness and strength for the structure or sub-zone of the structure under the given loading combination.

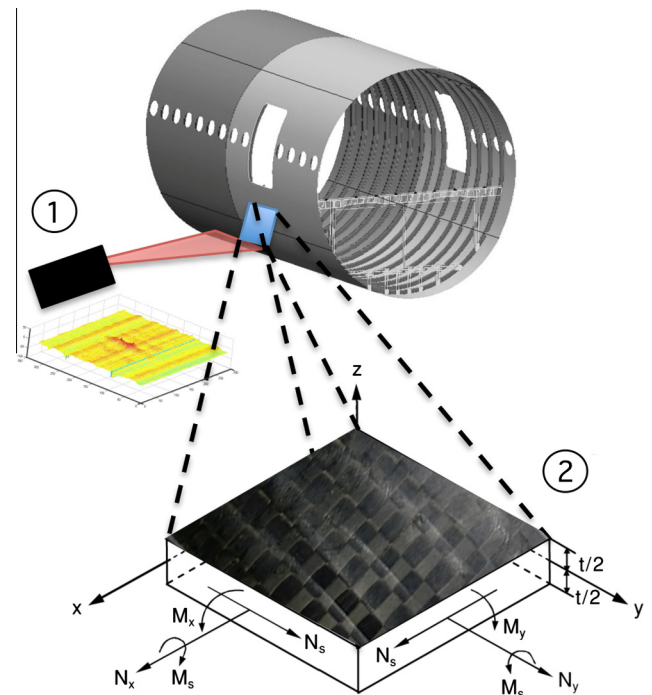


Fig. 1. Schematic of analysis framework. (1) Composite part is scanned with hyperspectral NIR imaging for surface resin pockets and wrinkles. (2) Progressive damage analysis is performed on sub-zone or entire structure if needed. (For interpretation of the references to color in this figure legend, the reader is referred to the web version of this article.)

3. Experiments and numerical simulations

3.1. Experimental method

The specimens in this study were fabricated from aerospace grade plain weave carbon-fiber epoxy fabric in prepreg (resin pre-impregnated fibers) preform. The prepreg is used for the specimens to reduce the variability in the processing since they produce more controlled fiber volume fractions and ply thicknesses. The fiber and epoxy used were a TORAY T700SC-12K-50C/#2510 plain weave fabric prepreg system [12]. The basic mechanical properties of the unidirectional tape prepreg system are tabulated in Table 1. The base procedure for fabrication of the test panel was modified to account for the wrinkling.

Several methods have been reported in the literature for creating the ply wrinkling profiles. Some of these profiles have been successfully replicated in a study on fabrication methods by using ply drop offs and transverse strips of composite material to trigger the waviness profile [13]. These methods have the drawback of inclusion of foreign material into the laminate. The use of metallic rods to initiate the out-of-plane waviness has been previously proposed [14,15]. In this procedure, the wrinkling is limited to the number of rods used and cannot usually generate large areas of waviness with random and non-uniform features. One study has shown how waviness can be created with oversized plies that conform to a given geometry [16]. In this study, the oversized ply method is used to create the random wrinkle distribution in the specimen. The oversized composite prepreg layers were packed into an aluminum mold. A silicon sheet of 5 mm thickness is applied over the composite to assist with consolidation. The laminates were cured using a 'hot-press' approach where uniform heat and pressure are applied per the recommended 121 $^{\circ}\text{C}$ (250 $^{\circ}\text{F}$) cure cycle. The NIR data was collected using a hyperspectral imaging system (Via-Spec Stage (MRC-920-044) with a SWIR hyper-

Table 1
Mechanical properties of the carbon/epoxy TORAY T700SC-12K-50C/#2510 Plain Weave Fabric [12].

E_1 GPa (Msi)	E_2 GPa (Msi)	ν_{12}	G_{12} GPa (Msi)	F_1^T GPa (ksi)	F_2^T GPa (ksi)	F_1^C GPa (ksi)	F_2^C GPa (ksi)	F_{12}^S GPa (ksi)	F_{13}^S GPa (ksi)
56.3 (8.16)	54.8 (7.96)	0.042	4.21 (0.611)	0.92 (133.1)	0.77 (112.4)	0.7 (102.8)	0.7 (101.9)	0.13 (19.23)	0.06 (8.7)

spectral camera (MRC-303-005-01), Middleton Spectral Vision, Middleton, WI).

The specimens were trimmed from a 304×304 mm (12×12 in.) panel cured using the process described above. The width of the specimen is 12.7 mm (0.50 in.) and the length is 68.6 mm (2.7 in.). Fig. 2 shows the panel after curing, with cross-sections from optical microscopy showing the random waviness profile spread over the specimen. The panel shows the successful creation of waviness zones that are randomly spread over the panel with different features with a particularly high waviness region as shown in Fig. 2. The high amplitude waviness zone itself also contains wrinkles with non-uniform features such as amplitude, length and number of successive waves. This is typical of waviness formed in the manufacturing environment as observed by the authors. The specimens from different areas representing different defect levels are tested using 3 point-flexure according to ASTM D7264 [17]. The extracted specimens were examined by optical microscopy and key features of the cross-section are shown in Table 2. Prior to sectioning the specimens, Step 1 of the procedure was implemented, in which the intact specimens were scanned using the near infrared hyperspectral imaging method.

3.2. Near infrared hyperspectral imaging

Near Infrared hyperspectral imaging is used to study the surface wrinkle distribution in the fabricated composite panel. In the near-infrared wavelength region the overtones and combination bands of the fundamental molecular vibrations are measured. The chemical specificity of such molecular vibrations allows the identification and quantification of materials and material mixtures. The specific absorption of the overtones and combination range is lower than that of the fundamental vibrations, thus materials, such as the excess resin on carbon composite parts can be investigated *in situ* without the need for dilution. The hyperspectral imaging method is similar to the conventional reflectance spectroscopy with a source illuminating the surface at an appropriate angle and optics detecting the reflected light within a particular wavelength range. With push-broom hyperspectral imaging, a camera integrated with a spectrograph is used to collect spectra at all locations on the sample one line at a time. Near-infrared light in the 1000–1700 nm range penetrates the resin and is scattered back from the carbon filaments so that light passes through the resin twice. The double transmission spectra detect the chemical signature of the resin, and the amplitudes of the spectral features are proportional to the resin depth at that point. The resin thickness is then calculated from the near infrared spectrum measured at each spatial point. Fig. 3 shows the reflectance spectra obtained on resin standards with different thicknesses that were made on test coupons to mimic the composite structure with resin on its surface.

The short wave infrared (SWIR) hyperspectral camera with full near-infrared wavelength range (1000–2500 nm) was used to scan the fabricated composite panels (Fig. 4). For the analysis in this paper, only the 1000–1700 nm region was used because the thicker resin causes optical saturation in the longer wavelength region. The authors also developed dedicated NIR resin measurement systems that display resin depths at various locations in real

time, using the method described above. Fig. 5 shows the detected and measured resin pockets on the composite panel, focusing on the region containing the waviness. Three distinct regions were selected from within the panel. In one region, there was a large amount of waviness with non-uniform wrinkle size and a random distribution. Three specimens with different levels of waviness have been cut from the waviness region of the panel and two specimens were cut from a region away from the high waviness zone. In the specimens extracted from the region with high waviness, significant spatial variability and non-uniformity of the wrinkling was observed. The waviness is non-uniform even within the same specimen. For example, Specimen 1 has a high-amplitude wrinkle on one side, which then degrades to a low-amplitude wrinkle on the other side. Similar variations are seen in other specimens to various degrees. The proposed model is capable of providing strength and stiffness estimation as the actual resin geometry and corresponding wrinkles were incorporated into the model.

3.3. Progressive damage modeling

The proposed modeling approach uses the high sensitivity of the hyperspectral NIR method with its capability to detect superficial resin pockets. These resin-filled surface pockets are directly correlated to regions where the fibers are wrinkled through the thickness of the composite laminate. This is confirmed by cross-section examination of specimens. In the progressive modeling process, the ply-by-ply finite element (FE) models are morphed into the actual geometry using the 3D surface resin thickness maps from the NIR hyperspectral images (Fig. 6). The mesh morphing process uses the 3D surface obtained from the NIR method to reconfigure the pristine mesh into a new mesh capturing the random and non-uniform waviness profiles. These structural morphing process steps were accomplished using a software program developed by the authors. In the morphed model, the damage mechanisms for the plain weave composite laminates are included (i.e. matrix cracking, fiber–matrix debonding, fiber fracture and interlaminar delamination). Due to the high transverse shear, translaminar failures may dominate the behavior of the flexure specimens. In order to investigate the relevant failure modes in this wrinkling analysis problem, the 3D Hashin–Puck's criteria [18,19] was employed with cohesive zone modeling for the interlayers [20]. The authors also incorporated a two-step, multi-scale progressive damage analysis based on the 3D Hashin criteria to study the damage behaviors of 2D plain weave composites under various uniaxial and biaxial loadings [21,22]. In the model, a direct method is used to model the interlaminar shear stress using solid brick elements. For the delamination failure modes, a cohesive surface interaction has been applied between layers from the top layer through the thickness. The interface in the cohesive zone model is modeled as a constitutive behavior specified by a traction–separation relationship. The derivation and finite element implementation of the cohesive damage model are described in [23]. Eight-node linear reduced integration brick with the reduced integration feature and hourglass control advantage (C3D8R) were used in separate layers. This feature provides a basis for accurate estimation of transverse shear stresses in a composite section where delaminations are possible.

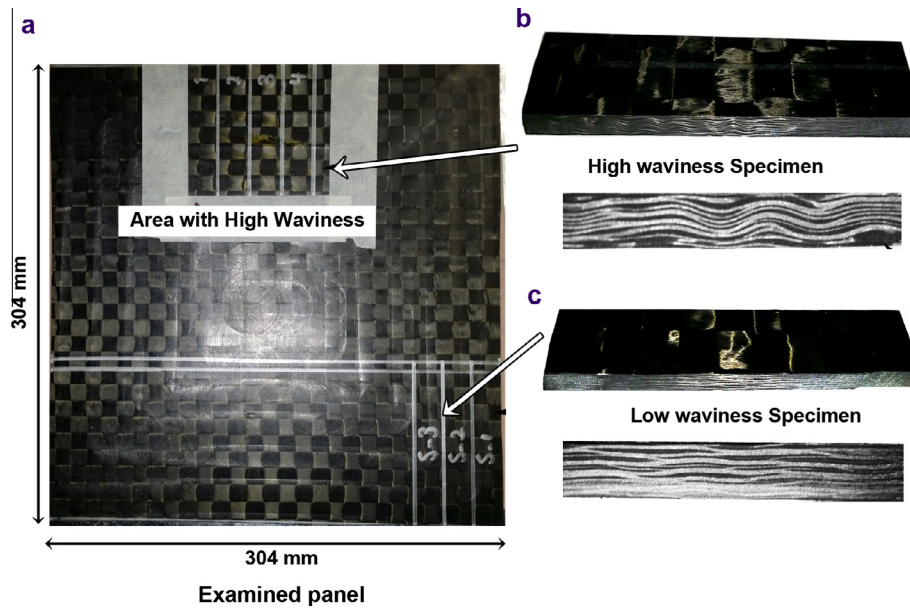


Fig. 2. Composite panel showing non-uniform ply waviness across different regions. (For interpretation of the references to color in this figure legend, the reader is referred to the web version of this article.)

Table 2
Wrinkle geometry of test specimens using optical microscopy.

Specimen ID ^a	Number of wrinkles (Right)	Number of wrinkles (Left)	Maximum amplitude (Right) (mm)	Maximum amplitude (Left) (mm)
Specimen 1	3	5	0.078	0.333
Specimen 2	6	3	0.382	0.184
Specimen 3	2	3	0.290	0.117
Specimen 4	~	~	0.020	0.031
Specimen 5	~	~	0.019	0.021

^a The flexure specimens are examined on the long ends. The amplitude of waviness in specimens 4 and 5 are considered the baseline for the woven material and are from properly consolidated regions with no resin pooling.

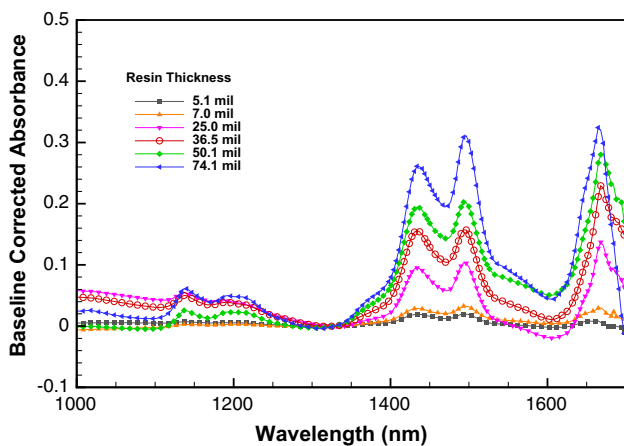


Fig. 3. Baseline corrected near infrared spectra (1000–1700 nm range) for a range of epoxy resin thicknesses. A calibration is created to correlate the measured absorbance with resin thickness at each scanning point. (For interpretation of the references to color in this figure legend, the reader is referred to the web version of this article.)

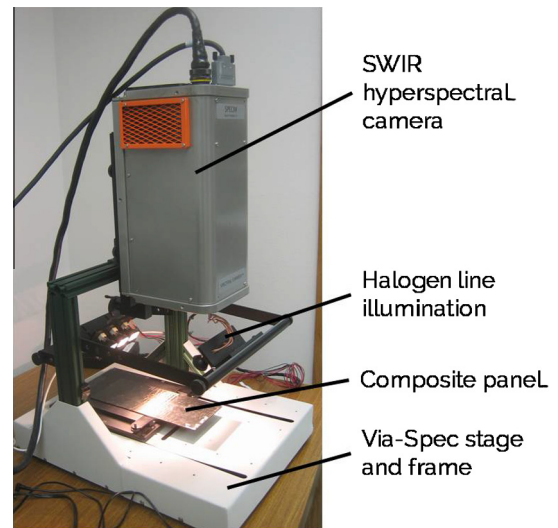


Fig. 4. Test setup for near infrared hyperspectral imaging of composite panel with spatially distributed non-uniform waviness. (For interpretation of the references to color in this figure legend, the reader is referred to the web version of this article.)

4. Results and discussion

A reasonable correlation is observed in the elastic and failure load between experiments and the progressive damage model of non-uniform waviness produced using the hyperspectral NIR method. The maximum load capacity of the specimens drops from 42% to 17% depending on the waviness profile and the location from which the specimen is extracted (Fig. 7). A remarkable correlation is observed between the model prediction and the failure loads of the extracted specimens. Specimens 1 to 3, which were extracted from a region having high waviness, have lower failure loads than Specimens 4 and 5, which were taken from regions having negligible waviness (Fig. 8). For the specimens from the high waviness zone, note the link between the maximum force values and the specimen geometry related to the location shown in Fig. 7.

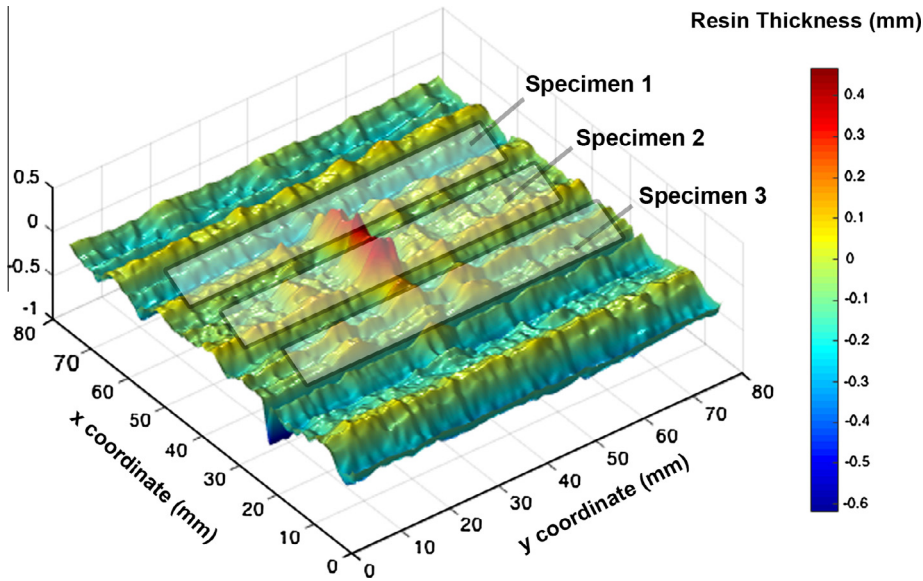


Fig. 5. The 3D surface map of resin pocket depth as measured by the near infrared hyperspectral imaging method. (For interpretation of the references to color in this figure legend, the reader is referred to the web version of this article.)

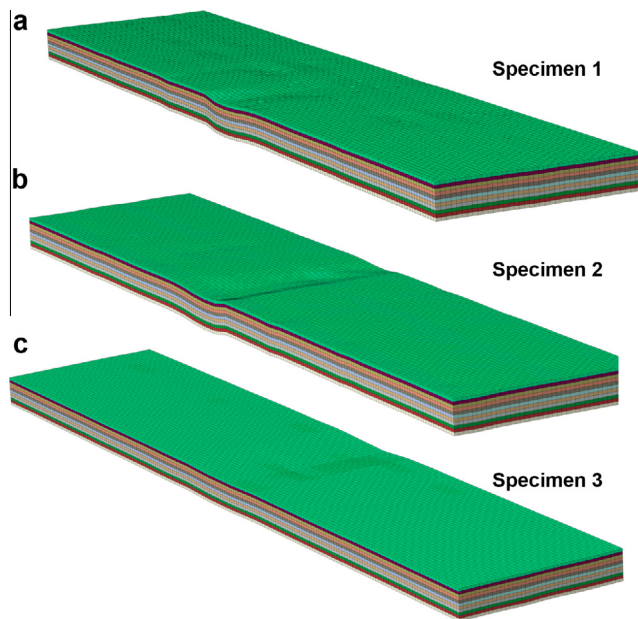


Fig. 6. Finite element meshes of specimens representing non-uniform spatially distributed wrinkling. (a) Specimen 1 containing distributed regions of waviness. (b) Specimen 2 containing severe non-uniform waviness. (c) Specimen 3 with low amounts of waviness. (For interpretation of the references to color in this figure legend, the reader is referred to the web version of this article.)

The series of experiments and simulations performed using this methodology also shed some light on damage mode transitions in the specimens related to the waviness profile and location. The progressive damage model failure modes observed show similar observations to the experimental results. The results are also consistent with previous studies in this area. The finite element method has been previously used to study the effects of wrinkles on composite properties [24]. Wisnom [25] used a non-linear finite element analysis showing the same mechanism of shear instability due to fiber waviness occurring under pure bending as under pure compressive loading. They showed that the maximum stress in bending was up to 73% higher than in compression. The results

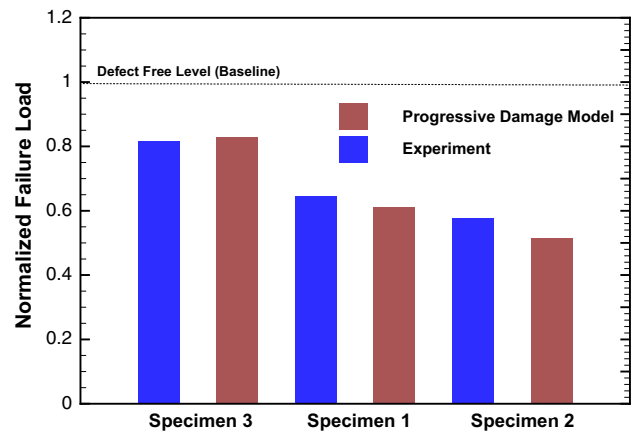


Fig. 7. Failure loads for specimens extracted from different regions in panel with spatially distributed non-uniform wrinkles. (For interpretation of the references to color in this figure legend, the reader is referred to the web version of this article.)

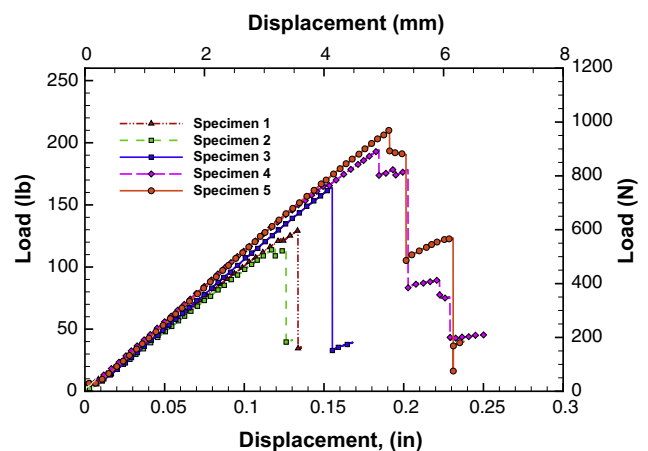


Fig. 8. Force versus displacement curves under 3-point flexural loading. (For interpretation of the references to color in this figure legend, the reader is referred to the web version of this article.)

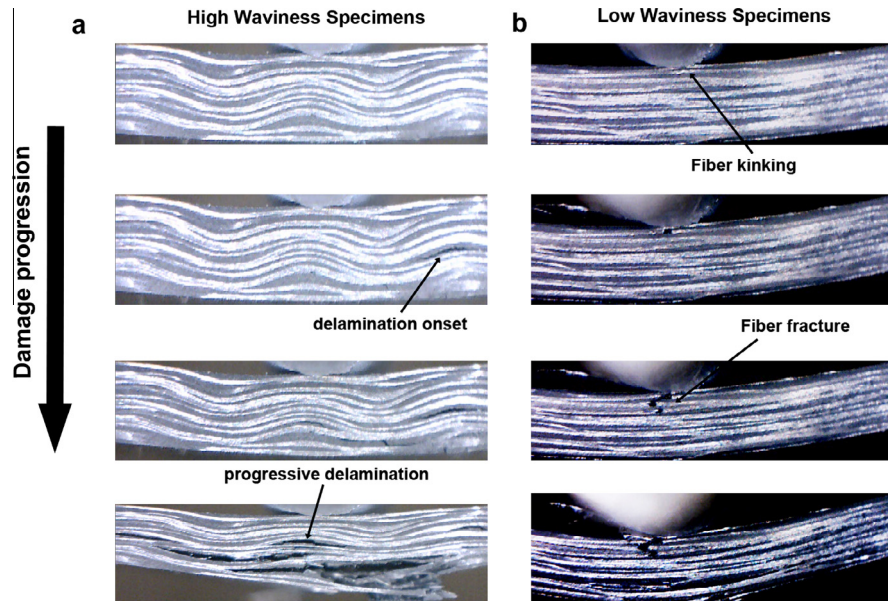


Fig. 9. Failure progressions using optical microscopy of (a) the high waviness amplitude specimen number 2 and (b) low waviness amplitude specimen number 3. (For interpretation of the references to color in this figure legend, the reader is referred to the web version of this article.)

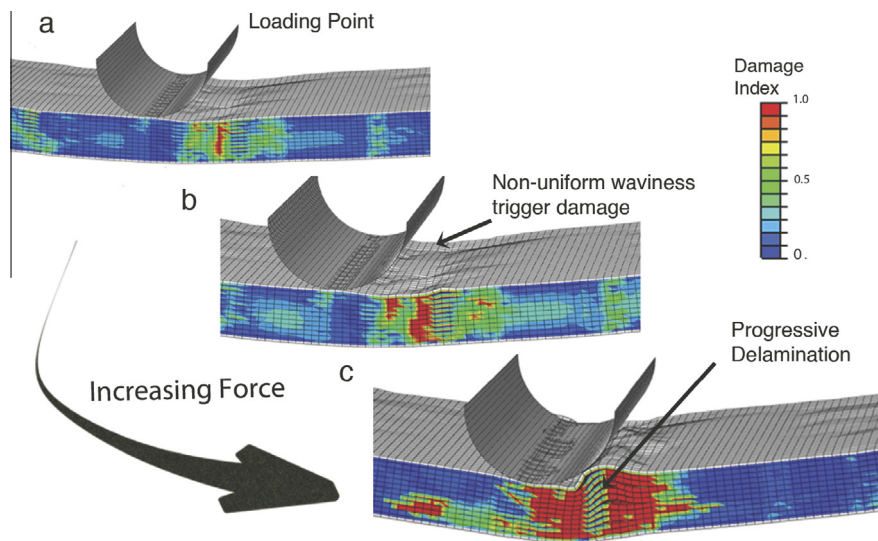


Fig. 10. Model results from Specimen 2 showing progressive growth of delamination under increasing force. In (a), the damage index represents regions where delamination has begun to occur. In (b) and (c) delamination grows from the initiation site occurring away from highest bending moment location under the load and affecting multiple plies. (For interpretation of the references to color in this figure legend, the reader is referred to the web version of this article.)

show that where failure is controlled by shear instability due to fiber waviness, compressive strength can be expected to be a function of stress gradient and therefore cannot be regarded as a true material property.

The hyperspectral imaging enhanced progressive damage models and the experiments show that delamination occurs at the highest fiber misalignment angle near the ply waviness apex. Delaminations appear as a result of kink band formation and interlaminar shear damage growing over the layers. Optical microscopy of the specimen edges during the flexural test shows two distinct failure mechanisms associated with varying regions of delamination.

In the specimen with the repeated high amplitude waviness profiles, the most dominating failure is delamination growth and propagation between the layers, particularly where the resin pocket is deepest. Large amounts of delamination occur before final failure occurs in the tension zone of the specimen. The fiber

kink band formation is confined to small zones. The onset of delamination is observed in both cases to occur at the point of highest fiber misalignment. The optical micrographs of Specimen 2 as it progresses to failure are shown in Fig. 9a. The domination of the delamination failure in the specimens with the higher amplitude can be understood with the fiber wrinkling leading to delamination at the resin pocket zone and finally to fiber fracture. Consequently, the spatial propagation of failure in these specimens starts from the highest waviness side and progresses across the width into the low waviness zone on the other edge.

For the specimen with a lower amount of waviness (Specimen 3), the interlaminar damage spreads through the plies, but is much more localized. This occurs since plies can take higher stresses and the shear can reach critical values before the onset of kink band formation and break. Localized and high transverse shear stress concentration points in the high waviness specimens lead to delamination failure at lower loads. The transverse shear stress is

also examined for the high and low waviness specimens. Fig. 10 shows the shear stress through the thickness at the load and at the point of highest fiber misalignment angle. The transverse shear stress is lower under the applied load than at the location of highest waviness. An interesting observation is that the results show a tension failure in the compression zone of the flexural specimen in the low-waviness specimens. The micro delamination of the upper layers of the low waviness specimen (Specimen 2) shows how the failure in the low waviness specimens is initiated by kink band formation and then the specimen breaks in a sublaminar zone (Fig. 9b). In Specimen 3, the top plies that are under compression show a narrow band of kinking where the matrix shear is dominant. The cracks grow at the fiber/matrix interface in the sublaminar region until the bottom fibers in the region experience a localized fracture in bending. Thus, in this specimen, the few wavy layers on the surface dominate the entire failure response of the specimen.

4.1. Limitations

A variety of factors can affect baseline and general shape of the NIR spectra used to generate the models. The most important factor is resin depth, but the surface finish on the resin, underlying fiber orientation, and the shape of the part being measured can also affect the results and thus must be considered in the construction of the calibration samples. The progressive modeling approach can be tedious and expensive computationally, but the measurement can be automated to produce site-based damage assessments.

5. Conclusions

The proposed method to predict the failure response of composite structures containing random and non-uniform out-of-plane waviness is demonstrated on laboratory size specimens. In the proposed method, NIR hyperspectral imaging is used to measure the actual surface resin profile and incorporate this shape to morph the mesh in a progressive damage based finite element model to predict the onset and propagation of damage in the composite structure. The proposed technique can be applied to a variety of composite structures where wrinkling of the plies can be related to small amounts of resin pooling on the surface. Specimens having random and non-uniform wrinkling profiles were fabricated and modeled using the progressive damage model with ply-by-ply layer definition.

The numerical results using the proposed method confirm the ability to predict strength reductions observed in the test specimens. They also provide important information about the failure progression and different failure modes. The proposed method is more accurate than previous approaches because of its capability to handle non-uniform and random wrinkle profiles. The continuum-based damage model with cohesive zone layers has demonstrated good agreement with the experimental results, but the proposed methodology does not preclude using other damage models.

The results show different failure modes with a transition from localized fiber kink band formation in a sublaminar region followed by fracture, to wide scale delamination depending on the location of the specimen. When the waviness was confined to a small sublaminar zone in the compression region, the fiber kink band formation and fracture were the primary mode of failure. When a specimen contained large amounts of waviness repeated through multiple layers of composite material, a transition to a delamination-based failure mode under flexure was observed. In the high waviness specimens, delamination initiates at the highest fiber misalignment points and results in narrow fiber kinking.

The results show that a more accurate structural assessment of the excess resin geometry on the surface of a composite structure

is possible by using chemometric processing techniques of spectra in the near infrared range to generate representative models capturing fiber undulations on the surface ranging from 125 to 2500 μm . The proposed method overcomes the limitations of current wrinkle assessment methods by connecting the high sensitivity near infrared hyperspectral measurements to direct structural models. The proposed approach can be used on composite articles in a production or service environment, thereby allowing for a cost-effective, rapid, and non-invasive full-field structural integrity evaluation.

Acknowledgement

We thank Kathy Speck for proofreading the final manuscript.

References

- [1] Chun HJ, Shin JY, Daniel IM. Nonlinear behavior of thick composites with uniform fiber waviness. *AIAA J* 2000;38(10):1949–55.
- [2] Chun HJ, Shin JY, Daniel IM. Effects of material and geometric nonlinearities on the tensile and compressive behavior of composite materials with fiber waviness. *Compos Sci Technol* 2001;61(1):125–34.
- [3] Hsiao HM, Daniel IM. Elastic properties of composites with fiber waviness. *Compos Part A – Appl Sci* 1996;27(10):931–41.
- [4] Potter K, Khan B, Wisnom M, Bell T, Stevens J. Variability, fibre waviness and misalignment in the determination of the properties of composite materials and structures. *Compos Part A – Appl Sci* 2008;39(9):1343–54.
- [5] Kugler D, Moon TJ. Identification of the most significant processing parameters on the development of fiber waviness in thin laminates. *J Compos Mater* 2002;36(12):1451–79.
- [6] Sutcliffe MPF, Lemanski SL, Scott AE. Measurement of fibre waviness in industrial composite components. *Compos Sci Technol* 2012;72(16):2016–23.
- [7] Nikishkov G, Nikishkov Y, Makeev A. Finite element mesh generation for composites with ply waviness based on X-ray computed tomography. *Adv Eng Softw* 2013;58:35–44.
- [8] Pain D, Drinkwater BW. Detection of fibre waviness using ultrasonic array scattering data. *J Nondestruct Eval* 2013;32(3):215–27.
- [9] Anastasi RF. Investigation of fiber waviness in a thick glass composite beam using THz NDE; 2008. p. 69340K-K-8.
- [10] Elhajjar R, Haj-Ali R, Wei B-S. An infrared thermoelastic stress analysis investigation for detecting fiber waviness in composite structures. *Polym-Plast Technol Eng* 2014;53(12):1251–8.
- [11] Shelley PH, Werner GJ, Vahey PG, Kemeny GJ, Groth GA, Stuessy G, et al. Near infrared imaging for measuring resin thickness on composites. In: *SAMPE annual conference*. Seattle (WA): Society for the Advancement of Material and Process Engineering; 2014.
- [12] Tomblin J, Sherraden J, Seneviratne W, Raju KS. Advanced general aviation transport experiments. A – basis and B – basis design allowables for epoxy – based prepreg TORAY T700SC-12K-50C/#2510 plain weave fabric. Wichita (KS): National Institute for Aviation Research Wichita State University; 2002.
- [13] Wang J, Potter K, Hazra K, Wisnom M. Experimental fabrication and characterization of out-of-plane fiber waviness in continuous fiber-reinforced composites. *J Compos Mater* 2012;46(17):2041–53.
- [14] Elhajjar RF, Shams SS. Compression testing of continuous fiber reinforced polymer composites with out-of-plane fiber waviness and circular notches. *Polym Testing* 2014;35:45–55.
- [15] El-Hajjar RF, Petersen DR. Gaussian function characterization of unnotched tension behavior in a carbon/epoxy composite containing localized fiber waviness. *Compos Struct* 2011;93(9):2400–8.
- [16] Bloom D, Wang J, Potter K. Damage progression and defect sensitivity: an experimental study of representative wrinkles in tension. *Compos B Eng* 2012.
- [17] ASTM D7264/D7264M-15. Standard test method for flexural properties of polymer matrix composite materials.
- [18] Hashin Z. Failure criteria for unidirectional fiber composites. *J Appl Mech* 1980;47(2):329–34.
- [19] Puck A, Schürmann H. Failure analysis of FRP laminates by means of physically based phenomenological models. *Compos Sci Technol* 2002;62(12):1633–62.
- [20] Shams S, Elhajjar R. Investigation into the effects of fiber waviness in standard notched composite specimens. *CEAS Aeronautical J* 2015:1–15.
- [21] Zhou Y, Lu Z, Yang Z. Progressive damage analysis and strength prediction of 2D plain weave composites. *Compos B Eng* 2013;47:220–9.
- [22] Abaqus. Abaqus 6-13.14. Dassault systems: Simulia; 2013.
- [23] Turon A, Camanho PP, Costa J, Dávila CG. A damage model for the simulation of delamination in advanced composites under variable-mode loading. *Mech Mater* 2006;38(11):1072–89.
- [24] Kyriakides S, Arseculeratne R, Perry E, Liechti K. On the compressive failure of fiber reinforced composites. *Int J Solids Struct* 1995;32(6):689–738.
- [25] Wisnom MR. The effect of fibre waviness on the relationship between compressive and flexural strengths of unidirectional composites. *J Compos Mater* 1994;28(1):66–76.